Phononic-waveguide-assisted steady-state entanglement of silicon-vacancy centers

Yi-Fan Qiao,[1] Hong-Zhen Li,[1] Xing-Liang Dong,[1] Jia-Qiang Chen,[1] Yuan Zhou,[2] and Peng-Bo Li[1,*]

[1]*Shaanxi Province Key Laboratory of Quantum Information and Quantum Optoelectronic Devices, Department of Applied Physics, Xi'an Jiaotong University, Xi'an 710049, China*

[2]*School of Science, Hubei University of Automotive Technology, Shiyan 442002, China*

(Received 4 December 2019; accepted 19 March 2020; published 13 April 2020)

Multiparticle entanglement is of great significance for quantum metrology and quantum information processing. We present here an efficient scheme for generating stable multiparticle entanglement in a solid-state setup, where an array of silicon-vacancy centers are embedded in a quasi-one-dimensional acoustic diamond waveguide. In this scheme, the continuum of phonon modes induces a controllable dissipative coupling among the SiV centers. We show that, by an appropriate choice of the distance between the SiV centers, the dipole-dipole interactions can be switched off due to destructive interference, thus realizing a Dicke superradiance model. This gives rise to an entangled steady state of SiV centers with high fidelities. The protocol provides a feasible setup for the generation of multiparticle entanglement in a solid-state system.

DOI: 10.1103/PhysRevA.101.042313

I. INTRODUCTION

Multiparticle entanglement has attracted great attention for its diverse applications in quantum metrology and quantum computing [1–10]. Great effort along this direction has led to plenty of proposals for generating entangled states with as many particles as possible [11–13], such as spin-squeezing states [14–16] and GHZ states [17–20]. So far, multiparticle entanglement has been realized involving up to 20 qubits in trapped-ion systems [21], and 12 qubits in superconducting circuits [22]. A dominant challenge to generate high-quality entangled states in the experiment comes from environment noise [23]. The particles inevitably interact with the environment, thus inducing the decoherence effect [24]. As a result, these entangled states are extremely fragile and easily destroyed. A feasible approach to solve this problem is using dissipation as a resource. Coupling to the environment drives the system to a steady state. By taking advantage of the dissipation, one can engineer a large variety of strongly correlated states in the steady state [25–37].

Color centers in diamond, such as germanium-vacancy (GeV) centers [38], nitrogen-vacancy (NV) centers [39–43], and silicon-vacancy (SiV) centers [44–47], play an important role in quantum science and technology [48–52]. Due to the high controllability and long coherence time [53–61], NV centers stand out among all kinds of solid-state systems. However, despite the impressive achievement with these solid-state systems, it is still challenging to realize quantum information processing with a large number of spins, due to the inherent weak coupling of NV spins to phonon modes and the difficulty in scaling to many spins. Recently, much attention has in particular been paid to the study of SiV centers [62–64]. The negatively charged SiV centers present strong zero-phonon line emission and narrow inhomogeneous broadening, which result from its inversion symmetry [65–67]. These characteristics have made SiV centers become an excellent candidate as quantum units, due to their favorable optical properties and flexible manipulation on the energy-level structures [68–70]. Moreover, it has been shown that SiV centers can realize strong and tunable coupling to phonons at the single quantum level [71–75].

In this paper, we propose an efficient scheme to generate steady-state entanglement of solid-state qubits with an array of SiV centers placed in a one-dimensional (1D) phononic diamond waveguide. A crucial advantage of utilizing the phononic waveguide is that SiV centers can be positioned at determined positions to modulate the phase difference [76,77]. In addition, the electronic ground states of SiV centers feature orbital degrees of freedom, which permit a direct and strong strain coupling to the phonon modes. Tailoring the system dissipation via the auxiliary external driven fields, the separated SiV centers are collectively coupled to the propagating phonon modes. Thus, we can engineer these SiV spins to a stable entangled state. By suitably choosing the distances of SiV centers, the dipole-dipole interactions will vanish due to destructive interferences [78–80], and we can achieve a dissipative Dicke superradiant [81] model in this setup [82,83]. This scheme provides a promising avenue for the generation of many-body entanglement in the steady state in solid-state setups.

II. MODEL

As depicted in Fig. 1(a), an array of N SiV centers are coupled to the phonon modes in a 1D diamond waveguide. The lattice distortion of longitudinal compression modes affects the electronic structure of the defect, which gives rise to strain coupling between the phonons and the orbital degrees of freedom of the SiV centers [71,74]. The Hamiltonian for the whole system is given by

$$\hat{H} = \hat{H}_{\mathrm{SiV}} + \hat{H}_{\mathrm{ph}} + \hat{H}_{\mathrm{strain}}. \tag{1}$$

*lipengbo@mail.xjtu.edu.cn

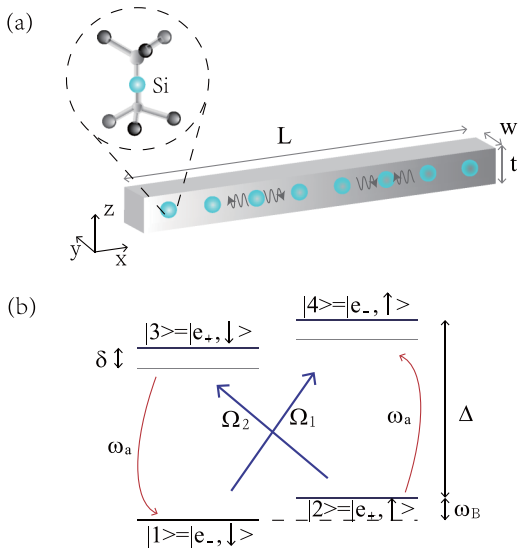

FIG. 1. (a) Sketch of an array of N SiV centers are embedded in a 1D phononic diamond waveguide at fixed positions x_j, with the uniform distance between two nearby SiV centers. The length, width, and thickness of the waveguide are L, w, and t, respectively. The orbital states of the centers are coupled via strain to a continuum of compression modes propagating along the waveguide (indicated by the curvy arrow). (b) Ground state of SiV centers. Two time-dependent microwave driving fields induce the Raman processes between $|3\rangle \leftrightarrow |2\rangle$ and $|4\rangle \leftrightarrow |1\rangle$.

The first term $\hat{H}_{\rm SiV}$ is the Hamiltonian of the N SiV centers. The second term $\hat{H}_{\rm ph}$ corresponds to the quantized Hamiltonian of the phononic waveguide modes. The last term $\hat{H}_{\rm strain}$ describes the strain coupling between the SiV centers and the phonon modes.

The SiV center in diamond is formed by a silicon atom and a split vacancy replacing two neighboring carbon atoms [see Fig. 1(a)] [66]. The Hamiltonian of a single SiV center includes three interaction parts: the spin-orbit coupling $\hat{H}_{\rm SO}$, the Jahn-Teller interaction $\hat{H}_{\rm JT}$, and the Zeeman interaction $\hat{H}_{\rm Z}$. Because the L_x and L_y components of the angular momentum $\vec{L}$ are zero in the basis spanned by the degenerate eigenstates $|e_x,\uparrow\rangle$, $|e_x,\downarrow\rangle$, $|e_y,\uparrow\rangle$, and $|e_y,\downarrow\rangle$, the spin-orbit interaction can be simplified to $\hat{H}_{\rm SO} = -\lambda_g L_z S_z$, where $\lambda_g = 2\pi \times 45$ GHz is the spin-orbit coupling [66]. In the presence of external magnetic fields, the Zeeman term is $\hat{H}_{\rm Z} = f\gamma_L L_z B_z + \gamma_S \vec{S}\cdot\vec{B}$, where γ_L and γ_S are the orbital and spin gyromagnetic ratios, respectively. The quenching factor $f \approx 0.1$ is caused by the Jahn-Teller coupling [66]. Assuming $\vec{B} = B_0\vec{e}_z$, we have the following Hamiltonian with the matrix form

$$\hat{H}_{\rm SiV} = -\lambda_g \begin{bmatrix} 0 & i \\ -i & 0 \end{bmatrix} \otimes \frac{1}{2}\begin{bmatrix} 1 & 0 \\ 0 & -1 \end{bmatrix} + \begin{bmatrix} \Upsilon_x & \Upsilon_y \\ \Upsilon_y & -\Upsilon_x \end{bmatrix} \otimes \mathbb{I} + f\gamma_L \begin{bmatrix} 0 & i \\ -i & 0 \end{bmatrix} \otimes B_0 \mathbb{I} + \gamma_S B_0 \mathbb{I} \otimes \frac{1}{2}\begin{bmatrix} 1 & 0 \\ 0 & -1 \end{bmatrix}. \quad (2)$$

Here, Υ_x and Υ_y are the distortions along x and y, and $\mathbb{I}$ denotes the 2×2 identity matrix. When neglecting the effect of the reduced orbital Zeeman interaction, the third term in Eq. (2) can be ignored [74]. Diagonalizing the above equation and in the case of $\Upsilon_{x,y} \ll \lambda_g$, we obtain the two lower eigenstates $|1\rangle \approx |e_-,\downarrow\rangle$, $|2\rangle \approx |e_+,\uparrow\rangle$, and two upper eigenstates $|3\rangle \approx |e_+,\downarrow\rangle$, $|4\rangle \approx |e_-,\uparrow\rangle$, with the splitting given by $\Delta = [\lambda_g^2 + 4(\Upsilon_x^2 + \Upsilon_y^2)]^{1/2} \approx 2\pi \times 46$ GHz [74]. Here, $|e_\pm\rangle = (|e_x\rangle \pm i|e_y\rangle)/\sqrt{2}$ are the eigenstates of the angular momentum L_z. We consider adding two time-dependent driving fields to induce the transition between $|1\rangle$ and $|4\rangle$, with the amplitude Ω_1 and frequency ω_1, and the transition between $|2\rangle$ and $|3\rangle$, with the amplitude Ω_2 and frequency ω_2. Thus, the Hamiltonian of a single SiV center driven by external fields can be described by

$$\hat{H}_{\rm SiV} = \omega_B|2\rangle\langle 2| + \Delta|3\rangle\langle 3| + (\Delta+\omega_B)|4\rangle\langle 4| + \frac{\Omega_1}{2}|1\rangle\langle 4|e^{i\omega_1 t} + \frac{\Omega_2}{2}|2\rangle\langle 3|e^{i\omega_2 t} + \text{H.c.}, \quad (3)$$

where $\omega_B = \gamma_s B_0$ is the Zeeman energy. The energy-level scheme and related transitions associated with $\hat{H}_{\rm SiV}$ are summarized in Fig. 1(b).

We now consider the Hamiltonian for the phonon modes in the diamond waveguide. For a 1D diamond phononic waveguide, the length, width, and thickness are labeled as L, w, and t, which satisfy the condition $L \gg wt$. For a linear isotropic medium, we can model the phonon modes as elastic waves with a displacement field $\vec{u}(\vec{r},t)$ [74]. Imposing the periodic boundary conditions and then quantizing the displacement field, we can obtain the quantized Hamiltonian [84] of the phonon modes

$$\hat{H}_{\rm ph} = \sum_{n,k} \hbar\omega_{n,k} a_{n,k}^\dagger a_{n,k}. \quad (4)$$

Here, $\omega_{n,k}$ is the frequency of phonon modes, with k the wave vector along the waveguide and n the branch index, and $a_{n,k}$ is the bosonic annihilation operator for the phonon mode. In addition, the quantized displacement field reads

$$\vec{u}(\vec{r}) = \sum_{n,k} \sqrt{\frac{\hbar}{2\rho V \omega_{n,k}}}\, \vec{u}_{n,k}^{\perp}(y,z)(a_{n,k}e^{ikx} + \text{H.c.}), \quad (5)$$

where ρ is the density, $V = Lwt$ is the volume of the waveguide, and $\vec{u}_{n,k}^{\perp}(y,z)$ is the transverse profile of the displacement field [74]. In Fig. 2, we summarize the simulated acoustic

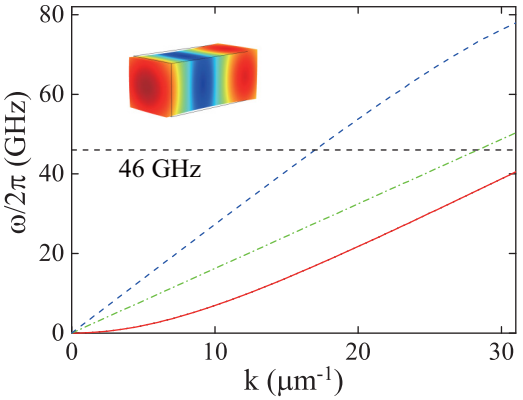

FIG. 2. Acoustic dispersion relation for a rectangular waveguide of width and thickness $w = t = 100$ nm. Inset shows normalized displacement profiles of symmetric phonons at 46 GHz.

dispersion relation and the displacement distribution for the waveguide with $w = t = 100$ nm.

We proceed to discuss the strain coupling between the SiV centers and the phononic waveguide modes. The change in Coulomb energy of electronic states due to a collective displacement of the defect atoms will induce strain coupling between these phonons and the orbital degrees of freedom of SiV centers [72]. When considering the small displacement of the defect atoms, the coupling between the phonon modes and the orbital degrees of freedom is linear in the Born-Oppenheimer approximation [71,72,74]. In this case, the strain coupling within the framework of linear elasticity theory can be given by

$$\hat{H}_{\text{strain}} = \epsilon_{E_{gx}}(\hat{L}_- + \hat{L}_+) - i\epsilon_{E_{gy}}(\hat{L}_- - \hat{L}_+), \tag{6}$$

where $\hat{L}_+ = \hat{L}_-^\dagger = |3\rangle\langle 1| + |2\rangle\langle 4|$ is the orbital raising operator within the ground state. The parameters $\epsilon_{E_{gx}}$ and $\epsilon_{E_{gy}}$ are

$$\begin{aligned} \epsilon_{E_{gx}} &= d(\epsilon_{xx} - \epsilon_{yy}) + f\epsilon_{zx}, \\ \epsilon_{E_{gy}} &= -2d\epsilon_{xy} + f\epsilon_{yz}, \end{aligned} \tag{7}$$

with ϵ_{ab} being the strain field tensor [72].

After taking Eqs. (5) and (7) into Eq. (6), we obtain the resulting strain coupling for N SiV centers:

$$\hat{H}_{\text{strain}} = \sum_{j,n,k} \left[g_{n,k}^j (J_+^j + J_-^j) a_{n,k} e^{ikx_j} + \text{H.c.} \right]. \tag{8}$$

Here $J_-^j = (J_+^j)^\dagger = |1\rangle_j\langle 3| + |2\rangle_j\langle 4|$ is the spin-conserving lowering operator and j labels the SiV center located at the position x_j. To get the right expression for the dipole-dipole interaction in the next part, it is crucial to keep the counter-rotating terms in the Hamiltonian for strain coupling [3]. After some derivation, the resulting coupling strength can be given as

$$g_{n,k}^j = d\sqrt{\frac{\hbar k^2}{2\rho V \omega_{n,k}}}\xi_{n,k}(y_j, z_j), \tag{9}$$

where $d/2\pi \approx 1$ PHz is the strain sensitivity [73,74]. Here, the dimensionless function $\xi_{n,k}(y,z)$ is related to the specific strain distribution. Putting everything together, the total Hamiltonian of the whole system is given by

$$\begin{aligned} \hat{H}_{\text{Total}} = &\sum_j \Big[\omega_B |2\rangle_j\langle 2| + \Delta |3\rangle_j\langle 3| + (\Delta + \omega_B)|4\rangle_j\langle 4| \\ &+ \frac{\Omega_1}{2}(|1\rangle_j\langle 4| e^{i\omega_1 t} + \text{H.c.}) + \frac{\Omega_2}{2}(|2\rangle_j\langle 3| e^{i\omega_2 t} + \text{H.c.}) \Big] \\ &+ \sum_{n,k} \omega_{n,k} a_{n,k}^\dagger a_{n,k} \\ &+ \sum_{j,n,k} [g_{n,k}^j (J_+^j + J_-^j) a_{n,k} e^{ikx_j} + \text{H.c.}]. \end{aligned} \tag{10}$$

III. STEADY-STATE ENTANGLEMENT

We use the quantum theory of damping in which the waveguide modes are treated as a reservoir. In this case, the phonon modes can be eliminated by using the Born-Markov approximation, giving rise to an effective master equation for the density operator $\hat{\rho}$, which describes the dissipative dynamics of the spin degrees of freedom. Starting from the model given in Eq. (10), we make a rotating transformation $H \to UHU^\dagger + iU^\dagger\dot{U}$ first, where the unitary operation $U = e^{i(\omega_1|4\rangle\langle 4| + \omega_2|3\rangle\langle 3|)t}$ [3]. The resulting Hamiltonian in the case of a single SiV center at the position $x_j = 0$ is

$$\begin{aligned} \hat{H} = &\sum_{n,k} \omega_{n,k} a_{n,k}^\dagger a_{n,k} + \omega_B |2\rangle\langle 2| + \Delta_2 |3\rangle\langle 3| + \Delta_1 |4\rangle\langle 4| \\ &+ \frac{\Omega_1}{2}(|1\rangle\langle 4| + \text{H.c.}) + \frac{\Omega_2}{2}(|2\rangle\langle 3| + \text{H.c.}) \\ &+ \sum_{n,k} g_{n,k} [(|3\rangle\langle 1| e^{i\omega_2 t} + |4\rangle\langle 2| e^{i\omega_1 t} + \text{H.c.}) a_{n,k} + \text{H.c.}], \end{aligned} \tag{11}$$

where $\Delta_1 = \Delta + \omega_B - \omega_1$ and $\Delta_2 = \Delta - \omega_2$. A crucial step to get the effective Hamiltonian is the adiabatic elimination of the excited states. Next, we apply the following canonical transformation $H \to e^{-S} H e^S$ [3,85], where

$$S = \frac{\Omega_1}{2\Delta_1}(|4\rangle\langle 1| - |1\rangle\langle 4|) + \frac{\Omega_2}{2\Delta_2}(|3\rangle\langle 2| - |2\rangle\langle 3|). \tag{12}$$

Note that this transformation is valid in the limit of $\Omega_1 \ll \Delta_1$ and $\Omega_2 \ll \Delta_2$. Keeping terms to the second order and neglecting the terms which are proportional to the excited-state populations, we obtain the effective Hamiltonian in the interaction picture with respect to $H_0 = \sum_{n,k} \omega_{n,k} a_{n,k}^\dagger a_{n,k} + \omega_B |2\rangle\langle 2|$:

$$\hat{H}_{\text{I}} = \alpha u(x_0, t)(D^+ e^{i\omega_a t} + \text{H.c.}), \tag{13}$$

with $u(x_0,t) = \sum_{n,k} g_{n,k}(a_{n,k} e^{-i\omega_a t} + \text{H.c.})$. $D^- = (D^+)^\dagger = u|1\rangle\langle 2| + \upsilon|2\rangle\langle 1|$ is a jump operator resulting from the cross radiative decay, with $u = \alpha^{-1}\Omega_2/2\Delta_2$ and $\upsilon = \alpha^{-1}\Omega_1/2\Delta_1$ satisfying the relation $u^2 - \upsilon^2 = 1$, and $\alpha^2 = (\Omega_1/2\Delta_1)^2 - (\Omega_2/2\Delta_2)^2$ is a normalization constant. This implies that these parameters can be written as $u = \cosh(r)$ and $\upsilon = \sinh(r)$. In this way, we can characterize the system by a single parameter, i.e., the squeezing parameter r. In addition, $\omega_a = \omega_1 - \omega_0 = \omega_2 + \omega_0$. This means the two decay channels denoted in red in Fig. 1(b) correspond to phonon emission with the same energy ω_a. Hence, the generalized interaction Hamiltonian in the situation of N SiV centers is

$$\hat{H}_{\text{I}} = \sum_j \alpha u(x_j, t)(D_j^+ e^{i\omega_a t} + \text{H.c.}). \tag{14}$$

We define ρ_S as the reduced density matrix for the SiV centers, and the dynamics of the SiV centers are governed by the Born-Markovian master equation [3,33,86,87]

$$\frac{d}{dt}\rho_S = \sum_{j,m} J_{j,m}[D_j^- \rho_S(t) D_m^+ - \rho_S(t) D_m^+ D_j^-] + \text{H.c.}, \tag{15}$$

where

$$J_{j,m} = \int_0^t dt (e^{-i\omega_a t} + e^{i\omega_a t}) \sum_{n,k} g_{n,k}^2 e^{-i\omega_{n,k} t} e^{ik(x_j - x_m)}. \tag{16}$$

This equation gives the dipole-dipole coupling strength between the SiV centers at positions x_j and x_m. In this process,

we assume the phonon field is in the vacuum. It means $\langle a^{\dagger}_{n,k} a_{n,k}\rangle = 0$.

To get the explicit expressions of $J_{j,m}$, we need some mathematical calculations. The first step is to replace the summation of k by an integral, and then transform the k integral into an energy integral by assuming the linear dispersion relationship $\omega_{n,k} = vk$ [3]. We finally have

$$J_{j,m} = \frac{\Gamma}{2} e^{i\omega_a |x_j - x_m|}, \tag{17}$$

where $\Gamma = \alpha^2 \gamma(\omega_a)$ is the collective decay rate, with $\gamma(\omega) = |g_{n,k}|^2 D(\omega)/\pi$, and $D(\omega) = (L/2\pi)|\partial_k \omega_{n,k}|$ the state density. Generally, the coupling between dipoles decays with the distance. One can find this conclusion easily from $J_{j,m}$. In this scheme, we choose the distance $x_n = n\lambda$ ($n \in \mathbb{Z}$) between two centers, and $\lambda = 2\pi/k$, with the purpose of canceling the dipole-dipole interaction by destructive interferences [3,78–80]. Eventually, we get the Dicke superradiant model [83] described by

$$\frac{d}{dt}\rho_S = \frac{\Gamma}{2}(D^- \rho_S D^+ - D^+ D^- \rho_S) + \text{H.c.}, \tag{18}$$

where $D^{+/-} = \sum_j D_j^{+/-}$ is the collective spin-squeezed operators. To quantify the degree of entanglement, we introduce the spin squeezing parameter $\xi^2_{R'}$:

$$\xi^2_{R'} = \frac{N(\Delta S_x)^2}{\langle S_y\rangle^2 + \langle S_z\rangle^2}, \tag{19}$$

where $S_\beta = \Sigma_j \sigma_j^\beta/2$ ($\beta = x, y, z$). We define the Pauli matrices $\sigma_z = |2\rangle\langle 2| - |1\rangle\langle 1|$, $\sigma_+ = |2\rangle\langle 1|$, and $\sigma_- = |1\rangle\langle 2|$. Spin squeezing is not only the measure of entanglement, but also has important applications in quantum metrology and quantum information processing [3,8,88,89]. The spin squeezing parameter $\xi^2_{R'}$ is proposed in Ref. [8], and it can be viewed as a generalization of the spin squeezing parameter ξ^2_R proposed by Wineland *et al.* in the study of spectroscopy [89,90]. When $\xi^2_{R'} < 1$, the states can be shown to be entangled. The definitions of spin squeezing are not uniform. Another spin squeezing definition is given by Kitagawa and Ueda [88,91]:

$$\xi^2_S = \frac{2}{N}\left[\langle S_1^2 + S_2^2\rangle - \sqrt{\langle S_1^2 - S_2^2\rangle^2 + \langle S_1 S_2 + S_2 S_1\rangle^2}\right], \tag{20}$$

where

$$\begin{aligned} S_1 &= S_y \cos\phi - S_x \sin\phi, \\ S_2 &= S_x \cos\theta \cos\phi + S_y \cos\theta \sin\phi - S_z \sin\theta, \\ \theta &= \arccos(\langle S_z\rangle / \sqrt{\langle S_x\rangle^2 + \langle S_y\rangle^2 + \langle S_z\rangle^2}), \\ \phi &= \arctan(\langle S_y\rangle / \langle S_x\rangle). \end{aligned} \tag{21}$$

These two spin squeezing definitions ξ^2_S and $\xi^2_{R'}$ are not equivalent. In Fig. 3 we plot the time evolution of the spin squeezing parameters for $N = 4$ to compare these two definitions. We find that $\xi^2_S < \xi^2_{R'}$, which is consistent with the conclusion in Ref. [92]. It has been proved that the spin squeezing parameters ξ^2_S and $\xi^2_{R'}$ are closely related to pairwise or many-body entanglement [8,76,92]. Note that such steady-state entanglement in Dicke superradiance has also been studied in a different context [91], which discussed an important aspect of the entanglement witness ξ^2_S. In this work, we choose $\xi^2_{R'}$ as the criterion to detect many body entanglement, and for simplification we drop the subscribe R' in the following.

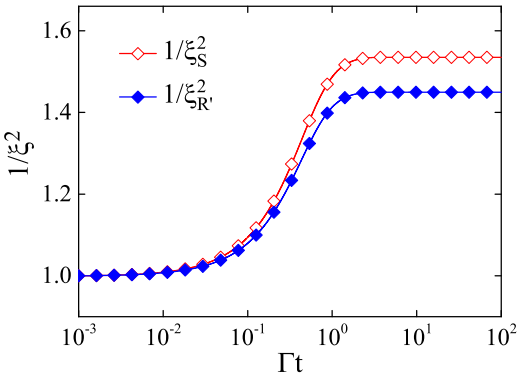

FIG. 3. Time evolution of the two spin squeezing parameters $1/\xi^2_{R'}$ and $1/\xi^2_S$ with $N = 4$, with $r = 0.2$.

We plot in Fig. 4 the time evolution of the squeezing parameter $1/\xi^2$. Here, we choose the value of the parameter $r = 0.2$, and $N = 2,\ 4,\ 6,\ 8$. For two SiV centers, the time for the system to reach the steady state is about $\Gamma t = 10$, and the value of the parameter $1/\xi^2$ is about 1.4. This means that these two centers are entangled. When the number of SiV centers $N = 4,\ 6,\ 8$, it only takes $\Gamma t < 1$ to realize the steady-state entanglement, and $1/\xi^2$ is about 1.5. The numerical result indicates that the degree of entanglement can be enhanced with an increasing number of SiV centers. Moreover, it takes less time for a large N to reach the steady state. Therefore, it will be more efficient to prepare the targeted states with a high fidelity with a large number of SiV centers.

We note that the Hamiltonian commutes with the total spin $\vec{S}^2$. This means, if the total spin of the system is given, the system will eventually reach a unique steady state regardless of the initial spin projection [32]. We assume that the initial state is $|\Psi_0\rangle = |S, m_s\rangle = |N/2, N/2\rangle$, and the system evolves within the sector $S = N/2$. We next check the time evolution of the squeezing parameter $1/\xi^2$ for different initial states in Fig. 5. One can find that all the squeezing parameters evolve

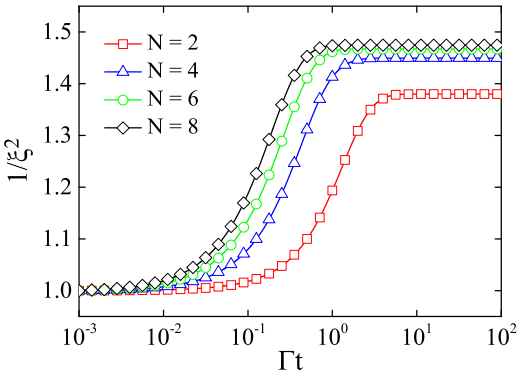

FIG. 4. Time evolution of the squeezing parameter $1/\xi^2$ with $N = 2, 4, 6, 8$.

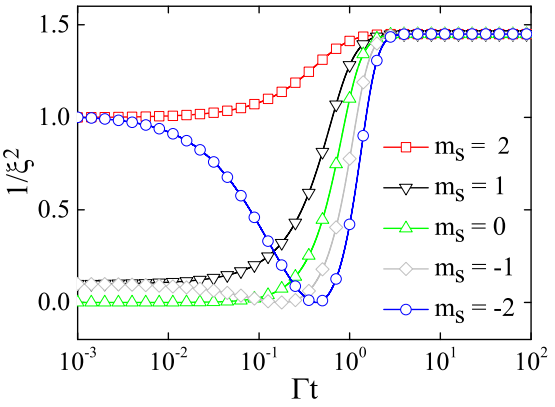

FIG. 5. Time evolution of the squeezing parameter $1/\xi^2$ for different initial states $|N/2, m_s\rangle$. Here the parameters are $N = 4$, and $r = 0.2$. Note that the steady state does not depend on the initial state in the subspace $S = N/2$.

asymptotically to the same stable value. This result agrees with what we discuss above.

Finally, in Fig. 6 we plot the calculation of the spin squeezing in the steady state as a function of the squeezing parameter r. When $N = 2$, the maximum value of $1/\xi^2$ rises to two when increasing the parameter r, and for $N = 8$, the maximum value of $1/\xi^2$ can reach five. From the figure, one can find an enhancement of the maximum value of the spin squeezing when increasing the number of the SiV centers.

For the realistic experimental condition in our scheme, we should take the dephasing rate Γ_D into consideration and add this inevitable adverse factor into our numerical simulation. According to Eq. (18), we can obtain

$$\frac{d}{dt}\rho_S = \Gamma\mathcal{D}[D^-]\rho_S + \Gamma_D \sum_j \mathcal{D}[\sigma_z^j]\rho_S, \tag{22}$$

where $\mathcal{D}[O]\rho = O\rho O^\dagger - 1/2(O^\dagger O\rho + \rho O^\dagger O)$, and $\Gamma_D = 1/2T_2$, with T_2^{-1} being the single spin dephasing rate [93–95].

We plot the time evolution of the spin squeezing parameter for $N = 2,\ 4,\ 6,\ 8$ spins in Fig. 7. Here, we still choose the value of the squeezing parameter as $r = 0.2$. We can obtain

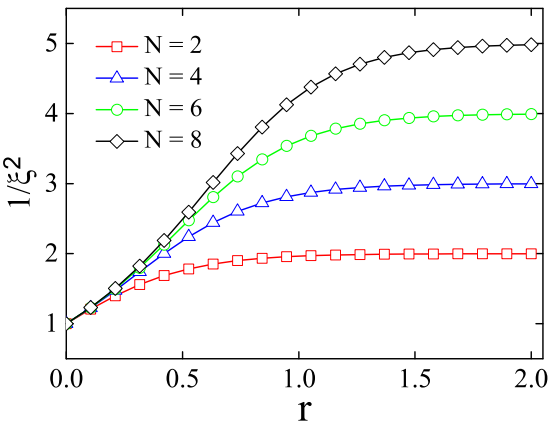

FIG. 6. Spin squeezing $1/\xi^2$ as a function of the squeezing parameter r at steady state, with different numbers of SiV centers ($N = 2,\ 4,\ 6,\ 8$).

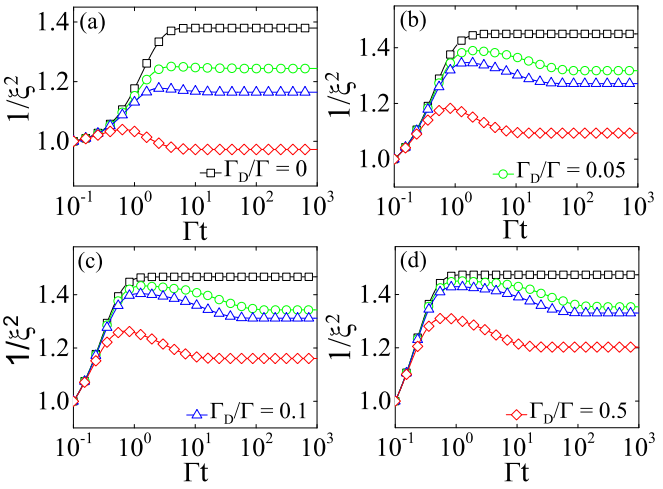

FIG. 7. Time evolution of the squeezing parameter $1/\xi^2$ for (a) $N = 2$, (b) $N = 4$, (c) $N = 6$, and (d) $N = 8$ in the presence of dephasing.

the maximal entanglement in the case of $\Gamma_D = 0$, which has been discussed above. For $\Gamma_D \neq 0$, the spin dephasing affects the steady-state entanglement, and the degree of entanglement will be reduced. As expected, this adverse effect will be significant as we increase Γ_D. In addition, the time interval for the system to reach the steady state entanglement is negatively related to Γ_D. As illustrated in Fig. 7, for a large N, as long as we take a much larger dephasing rate, the time interval for reaching the steady entanglement will be shorter during this dynamical evolution process. In Fig. 8, we present the calculation of the spin squeezing in the steady state as a function of the squeezing parameter r for $N = 2,\ 4,\ 6,\ 8$. The dephasing effect competes with the collective decay, which results in an optimal r to generate the maximal steady-state entanglement. And this optimal spin parameter r is inversely related to the dephasing rate Γ_D.

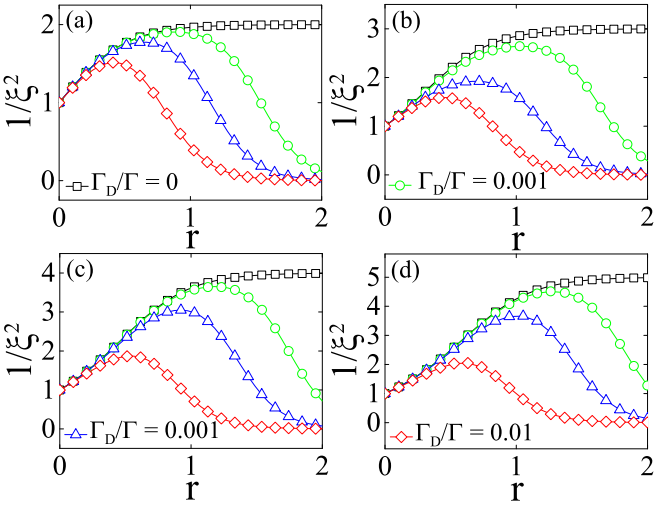

FIG. 8. The degree of entanglement as a function of the squeezing parameter r for (a) $N = 2$, (b) $N = 4$, (c) $N = 6$, and (d) $N = 8$ in the presence of dephasing.

IV. THE FEASIBILITY OF THIS SCHEME

In this work, we propose a spin-phononic waveguide system, where separated SiV centers are coupled by quantized phonon modes of a one-dimensional diamond waveguide. Based on state-of-the-art nanofabrication techniques, several experiments have demonstrated the generation of SiV center arrays through ion implantation techniques [96,97]. For instance, three arrays of SiV centers are integrated into the diamond cantilever, and are placed at determined position to control the interaction of its spins with the thermal bath in Ref. [73]. In general, the proposed setup can be implemented experimentally where an array of SiV centers are embedded in a 1D diamond waveguide.

For the phonon diamond waveguide, the length and cross section are $L = 100\ \mu$m and $A = 100 \times 100\ \text{nm}^2$. In addition, the material properties of the diamond waveguide are $\rho = 3500\ \text{kg/m}^3$, $E = 1050$ GPa, and $\nu = 0.2$. In this case, the group velocity along the waveguide is $v = 1.71 \times 10^4$ m/s, and the single SiV center can couple to the phonon mode with a strength $g/2\pi = 4$ MHz.

For the SiV center in diamond, the ground-state splitting is about $\Delta/2\pi = 46$ GHz. And the transitions between $|3\rangle \leftrightarrow |2\rangle$ and $|4\rangle \leftrightarrow |1\rangle$ can be implemented by using a microwave field [74] or via an equivalent optical Raman process [74], which has already been carried out experimentally. In our model, the precise location of the SiV centers is required with the purpose of canceling the dipole-dipole interactions by destructive interference. The diamond waveguide permits us to place the SiV centers permanently at the position $x_n = n\lambda$ [3], where $\lambda \approx 200$ nm is the phonon wavelength. Under this consideration, a waveguide with $L = 100\ \mu$m can contain 500 SiV centers, approximately.

At 100 mK temperature, the spin dephasing time of a single SiV center is about $\gamma_s/2\pi = 100$ Hz. Thus the spin coherence time is $T_2 \sim 10$ ms [68]. Assuming $\Omega_1/2\pi,\ \Omega_2/2\pi \approx 10$ MHz and $\Delta_1/2\pi,\ \Delta_2/2\pi \approx 100$ MHz, the effective decay rate is $\Gamma/2\pi = 160$ kHz. According to Fig. 4, the time for the system to reach the steady-state entanglement is about $\Gamma t \lesssim 10$, i.e., $T \approx 10\ \mu$s, which is much shorter than the spin coherence time T_2. This shows that the condition for the steady-state entanglement can be reached.

V. CONCLUSION

In conclusion, we have proposed a scheme to generate multiparticle entanglement of solid-state qubits by embedding an array of SiV centers in a one-dimensional phononic diamond waveguide. We study the efficient coupling between the SiV centers and the phononic waveguide modes. The unique structure of the waveguide allows us to switch off the dipole-dipole interactions via destructive interference by appropriately choosing the distance between nearby SiV centers. We can achieve the Dicke superradiant model under appropriate external driving fields. We also discuss the degree of entanglement in the presence of realistic decoherence. This scheme may provide a realistic and feasible platform for quantum information processing with spins and phonons in a solid-state system.

ACKNOWLEDGMENTS

This work is supported by the National Natural Science Foundation of China under Grant No. 11774285, and Natural Science Basic Research Program of Shaanxi (Program No. 2020JC-02).

APPENDIX A: THE HAMILTONIAN OF SIV CENTERS

The detailed derivation for the Hamiltonian of SiV centers has been discussed in Refs. [66,72,74]. Here we follow their discussions and present the key results. We start from the Hamiltonian [Eq. (2) in the main text], which is in the basis spanned by the degenerate eigenstates $|e_x,\uparrow\rangle$, $|e_x,\downarrow\rangle$, $|e_y,\uparrow\rangle$, and $|e_y,\downarrow\rangle$,

$$\hat{H}_{\text{SiV}} = -\lambda_g \begin{bmatrix} 0 & i \\ -i & 0 \end{bmatrix} \otimes \frac{1}{2}\begin{bmatrix} 1 & 0 \\ 0 & -1 \end{bmatrix} + \begin{bmatrix} \Upsilon_x & \Upsilon_y \\ \Upsilon_y & -\Upsilon_x \end{bmatrix} \otimes \mathbb{I} + f\gamma_L \begin{bmatrix} 0 & i \\ -i & 0 \end{bmatrix} \otimes B_0 \mathbb{I} + \gamma_S B_0 \mathbb{I} \otimes \frac{1}{2}\begin{bmatrix} 1 & 0 \\ 0 & -1 \end{bmatrix}. \quad \text{(A1)}$$

After some simplifications and neglecting the effect of the reduced orbital Zeeman interaction, we obtain the total Hamiltonian of SiV centers,

$$\hat{H}_{\text{SiV}} = \begin{bmatrix} \frac{1}{2}\gamma_S B_0 + \Upsilon_x & 0 & -\frac{i}{2}\lambda_g + \Upsilon_y & 0 \\ 0 & -\frac{1}{2}\gamma_S B_0 + \Upsilon_x & 0 & \frac{i}{2}\lambda_g + \Upsilon_y \\ \frac{i}{2}\lambda_g + \Upsilon_y & 0 & \frac{1}{2}\gamma_S B_0 - \Upsilon_x & 0 \\ 0 & -\frac{i}{2}\lambda_g + \Upsilon_y & 0 & -\frac{1}{2}\gamma_S B_0 - \Upsilon_x \end{bmatrix}. \quad \text{(A2)}$$

Diagonalizing the above matrix, we have the eigenenergies

$$E_{3,1} = -\frac{1}{2}\gamma_S B_0 \pm \sqrt{\Upsilon^2 + \frac{1}{4}\lambda_g^2},$$
$$E_{4,2} = \frac{1}{2}\gamma_S B_0 \pm \sqrt{\Upsilon^2 + \frac{1}{4}\lambda_g^2}. \quad \text{(A3)}$$

Here, $\Upsilon = (\Upsilon_x^2 + \Upsilon_y^2)^{1/2}$ is the Jahn-Teller coupling strength. It has been shown that the spin-orbit interaction and the Jahn-Teller effect both lift the orbital degeneracy of ground states of SiV centers [66]. Besides, the spin-orbit coupling strength $\lambda_g \gg \Upsilon_{x,y}$. We thus neglect the Jahn-Teller effect on the orbital states. In this case, the corresponding normalized eigenstates are

$$|1\rangle \approx (|e_x,\downarrow\rangle - i|e_y,\downarrow\rangle)/\sqrt{2} = |e_-,\downarrow\rangle,$$
$$|2\rangle \approx (|e_x,\uparrow\rangle + i|e_y,\uparrow\rangle)/\sqrt{2} = |e_+,\uparrow\rangle,$$
$$|3\rangle \approx (|e_x,\downarrow\rangle + i|e_y,\downarrow\rangle)/\sqrt{2} = |e_+,\downarrow\rangle,$$
$$|4\rangle \approx (|e_x,\uparrow\rangle - i|e_y,\uparrow\rangle)/\sqrt{2} = |e_-,\uparrow\rangle. \quad \text{(A4)}$$

After shifting the whole energy level of SiV centers, i.e., choosing $E_1 = 0$, we then have the Hamiltonian form (3) in the main text.

APPENDIX B: THE QUANTIZATION OF THE PHONON WAVEGUIDE MODES

We follow the discussion in Ref. [74] to obtain the key results on the quantization of the phonon waveguide modes. We consider a 1D diamond waveguide with a cross section A and a length $L \gg A$. The phonon modes can be viewed as elastic waves in the elastic theory, characterized by the displacement field $\vec{u}(\vec{r}, t)$ [74]. For a linear isotropic medium, the displacement field is described by the equation of motion

$$\rho \frac{\partial^2}{\partial t^2}\vec{u} = (\lambda + \mu)\vec{\nabla}(\vec{\nabla}\cdot\vec{u}) + \mu\vec{\nabla}^2\vec{u}, \tag{B1}$$

where $\rho = 3500\ \mathrm{kg/m^3}$ is the mass density of diamond waveguide, and λ and μ are the Lamé constants,

$$\lambda = \frac{\nu E}{(1+\nu)(1-2\nu)}, \quad \mu = \frac{E}{2(1+\nu)}. \tag{B2}$$

For diamond, we use the Young's modulus $E = 1050$ GPa and the Poisson ratio $\nu = 0.2$.

Under the periodic boundary conditions $k = 2\pi m/L$ ($m \in \mathbb{Z}$), the solution of Eq. (B1) is given by

$$\vec{u}(\vec{r}, t) = \frac{1}{\sqrt{2}}\sum_{n,k}\vec{u}^{\perp}_{n,k}(y,z)[A_{n,k}(t)e^{ikx} + \text{c.c.}]. \tag{B3}$$

Here, amplitudes $A_{n,k}(t)$ satisfy the oscillating equation $\ddot{A}_{n,k}(t) + \omega^2_{n,k}A_{n,k}(t) = 0$ [74]. The value of the mode frequencies $\omega_{n,k}$ and the transverse-mode profile $\vec{u}^{\perp}_{n,k}(y,z)$ can be obtained from numerical solutions, and $\vec{u}^{\perp}_{n,k}(y,z)$ are orthogonal and normalized to

$$\frac{1}{A}\int dydz\vec{u}^{\perp}_{n,k}(y,z)\cdot\vec{u}^{\perp}_{m,k}(y,z) = \delta_{nm}. \tag{B4}$$

The quantization of the displacement field is similar to the electromagnetic field in quantum optics. Taking the equivalence

$$A_{n,k} \to \sqrt{\frac{\hbar}{\rho V\omega_{n,k}}}a^{\dagger}_{n,k}, \quad A^{*}_{n,-k} \to \sqrt{\frac{\hbar}{\rho V\omega_{n,k}}}a_{n,-k}, \tag{B5}$$

we can obtain the quantized displacement field [74]

$$\vec{u}(\vec{r}\,) = \sum_{n,k}\sqrt{\frac{\hbar}{2\rho V\omega_{n,k}}}\vec{u}^{\perp}_{n,k}(y,z)(a_{n,k}e^{ikx} + a^{\dagger}_{n,k}e^{-ikx}), \tag{B6}$$

and the quantized phonon modes

$$\hat{H}_{\text{ph}} = \sum_{n,k}\hbar\omega_{n,k}a^{\dagger}_{n,k}a_{n,k}. \tag{B7}$$

APPENDIX C: STRAIN COUPLING

We follow the discussion in Ref. [74] to obtain the key results on strain coupling between SiV centers and phononic waveguide modes. For small displacements and in the Born-Oppenheimer approximation, the strain coupling within the framework of linear elasticity theory can be given by

$$\hat{H}_{\text{strain}} = \sum_{ij}V_{ij}\epsilon_{ij}. \tag{C1}$$

Here, i, j label the coordinate axes. V_{ij} is an operator acting on the electronic states of the SiV defect and ϵ_{ij} is the strain field tensor [56]. The local strain tensor is defined as

$$\epsilon_{ij} = \frac{1}{2}\left(\frac{\partial u_i}{\partial x_j} + \frac{\partial u_j}{\partial x_i}\right), \tag{C2}$$

with u_x (u_y, u_z) representing the quantized displacement field along x (y, z) at the position of the SiV center. We assume the axes as shown in Fig. 1(a). By projecting the strain tensor onto the irreducible representation of D_{3d}, the Hamiltonian can be rewritten in terms of the electronic states of the SiV defect,

$$\hat{H}_{\text{strain}} = \sum_{r}V_r\epsilon_r, \tag{C3}$$

where r runs over the irreducible representations. It can be shown that the only contributing representations are the one-dimensional representation A_{1g} and the two-dimensional representation E_g. Due to the inversion symmetry, the ground states of the SiV center transform as E_g, and the excited states transform as E_u. Therefore, one can find that strain can couple independently to orbital within the ground and excited manifolds. Limiting only to the ground state, the terms in Eq. (C3) are given by

$$\begin{aligned}\epsilon_{A_{1g}} &= t_{\perp}(\epsilon_{xx} + \epsilon_{yy}) + t_{\parallel}\epsilon_{zz},\\ \epsilon_{E_{gx}} &= d(\epsilon_{xx} - \epsilon_{yy}) + f\epsilon_{zx},\\ \epsilon_{E_{gy}} &= -2d\epsilon_{xy} + f\epsilon_{yz},\end{aligned} \tag{C4}$$

where $t_{\perp}$, $t_{\parallel}$, d, f are four strain-susceptibility parameters. Furthermore, the effects of these strain components on the electronic states are given by

$$\begin{aligned}V_{A_{1g}} &= |e_x\rangle\langle e_x| + |e_y\rangle\langle e_y|,\\ V_{E_{gx}} &= |e_x\rangle\langle e_x| - |e_y\rangle\langle e_y|,\\ V_{E_{gy}} &= |e_x\rangle\langle e_y| + |e_y\rangle\langle e_x|.\end{aligned} \tag{C5}$$

As the energy shift of all ground states induced by symmetry local distortions is equal, it can be neglected. Finally, we write the strain Hamiltonian by using the basis spanned by the eigenstates of the spin-orbit coupling $|e_+\rangle$, and $|e_-\rangle$:

$$\hat{H}_{\text{strain}} = \epsilon_{E_{gx}}(\hat{L}_- + \hat{L}_+) - i\epsilon_{E_{gy}}(\hat{L}_- - \hat{L}_+), \tag{C6}$$

where $\hat{L}_+ = \hat{L}^{\dagger}_- = |3\rangle\langle 1| + |2\rangle\langle 4|$. By decomposing the local displacement field in terms of the vibrational eigenmodes, the resulting strain coupling can be written as

$$\hat{H}_{\text{strain}} = \sum_{n,k}[g_{n,k}(J_+ + J_-)a_{n,k}e^{ikx} + \text{H.c.}], \tag{C7}$$

with the coupling strength having the form

$$\begin{aligned}g_{n,k} = g_0\frac{1}{|k|}\Bigg[&\left(iku^{\perp,x}_{n,k} + ik\frac{f}{d}\frac{u^{\perp,z}_{n,k}}{2} + \frac{f}{d}\frac{\partial_z u^{\perp,x}_{n,k}}{2} - \partial_y u^{\perp,y}_{n,k}\right)\\ &- i\left(iku^{\perp,y}_{n,k} + \frac{f}{d}\frac{\partial_y u^{\perp,z}_{n,k}}{2} + \frac{\partial_z u^{\perp,y}_{n,k}}{2} + \partial_y u^{\perp,x}_{n,k}\right)\Bigg],\end{aligned} \tag{C8}$$

where $g_0 = (\hbar k^2 d^2/2\rho V\omega_{n,k})^{1/2}$.

[1] A. Micheli, D. Jaksch, J. I. Cirac, and P. Zoller, Many-particle entanglement in two-component Bose-Einstein condensates, Phys. Rev. A **67**, 013607 (2003).

[2] P. Xu, S. Yi, and W. Zhang, Efficient Generation of Many-Body Entangled States by Multilevel Oscillations, Phys. Rev. Lett. **123**, 073001 (2019).

[3] A. González-Tudela and D. Porras, Mesoscopic Entanglement Induced by Spontaneous Emission in Solid-State Quantum Optics, Phys. Rev. Lett. **110**, 080502 (2013).

[4] G.-Q. Liu, Y.-R. Zhang, Y.-C. Chang, J.-D. Yue, H. Fan, and X.-Y. Pan, Demonstration of entanglement-enhanced phase estimation in solid, Nat. Commun. **6**, 6726 (2015).

[5] P.-B. Li and F.-L. Li, Deterministic generation of multiparticle entanglement in a coupled cavity-fiber system, Opt. Express **19**, 1207 (2011).

[6] E. Y.-Z. Tan, D. Kaszlikowski, and L. C. Kwek, Entanglement witness via symmetric two-body correlations, Phys. Rev. A **93**, 012341 (2016).

[7] M. B. Plenio and S. F. Huelga, Entangled Light from White Noise, Phys. Rev. Lett. **88**, 197901 (2002).

[8] A. Sørensen, L.-M. Duan, J. I. Cirac, and P. Zoller, Many-particle entanglement with Bose-Einstein condensates, Nature (London) **409**, 63 (2001).

[9] M. B. Plenio, S. F. Huelga, A. Beige, and P. L. Knight, Cavity-loss-induced generation of entangled atoms, Phys. Rev. A **59**, 2468 (1999).

[10] G. Tóth, C. Knapp, O. Gühne, and H. J. Briegel, Spin squeezing and entanglement, Phys. Rev. A **79**, 042334 (2009).

[11] Y. Wang, Y. Li, Zhang-qi Yin, and B. Zeng, 16-qubit IBM universal quantum computer can be fully entangled, npj Quantum Inf. **4**, 46 (2018).

[12] X.-L. Wang, L.-K. Chen, W. Li, H.-L. Huang, C. Liu, C. Chen, Y.-H. Luo, Z.-E. Su, D. Wu, Z.-D. Li, H. Lu, Y. Hu, X. Jiang, C.-Z. Peng, L. Li, N.-L. Liu, Y.-Ao Chen, C.-Y. Lu, and J.-W. Pan, Experimental Ten-Photon Entanglement, Phys. Rev. Lett. **117**, 210502 (2016).

[13] C. Song, K. Xu, W. Liu, Chui-ping Yang, S.-B. Zheng, H. Deng, Q. Xie, K. Huang, Q. Guo, L. Zhang, P. Zhang, D. Xu, D. Zheng, X. Zhu, H. Wang, Y.-A. Chen, C.-Y. Lu, S. Han, and J.-W. Pan, 10-Qubit Entanglement and Parallel Logic Operations with A Superconducting Circuit, Phys. Rev. Lett. **119**, 180511 (2017).

[14] K. Xia and J. Twamley, Generating spin squeezing states and Greenberger-Horne-Zeilinger entanglement using a hybrid phonon-spin ensemble in diamond, Phys. Rev. B **94**, 205118 (2016).

[15] L. Dellantonio, S. Das, J. Appel, and A. S. Sørensen, Multipartite entanglement detection with nonsymmetric probing, Phys. Rev. A **95**, 040301(R) (2017).

[16] M. S. Rudner, L. M. K. Vandersypen, V. Vuletić, and L. S. Levitov, Generating Entanglement and Squeezed States of Nuclear Spins in Quantum Dots, Phys. Rev. Lett. **107**, 206806 (2011).

[17] F. Fröwis and W. Dür, Stable Macroscopic Quantum Superpositions, Phys. Rev. Lett. **106**, 110402 (2011).

[18] T. Li, A. Miranowicz, K. Xia, and F. Nori, Resource-efficient analyzer of Bell and Greenberger-Horne-Zeilinger states of multiphoton systems, Phys. Rev. A **100**, 052302 (2019).

[19] T. Li, Z. Wang, and K. Xia, Multipartite quantum entanglement creation for distant stationary systems, Opt. Express **28**, 1316 (2020).

[20] R.-H. Zheng, Y.-H. Kang, D. Ran, Z.-C. Shi, and Y. Xia, Deterministic interconversions between the Greenberger-Horne-Zeilinger states and the w states by invariant-based pulse design, Phys. Rev. A **101**, 012345 (2020).

[21] N. Friis, O. Marty, C. Maier, C. Hempel, M. Holzäpfel, P. Jurcevic, M. B. Plenio, M. Huber, C. Roos, R. Blatt, and B. Lanyon, Observation of Entangled States of A Fully Controlled 20-Qubit System, Phys. Rev. X **8**, 021012 (2018).

[22] M. Gong, M.-C. Chen, Y. Zheng, S. Wang, C. Zha, H. Deng, Z. Yan, H. Rong, Y. Wu, S. Li, F. Chen, Y. Zhao, F. Liang, J. Lin, Y. Xu, C. Guo, L. Sun, A. D. Castellano, H. Wang, C. Peng, C.-Y. Lu, X. Zhu, and J.-W. Pan, Genuine 12-Qubit Entanglement on a Superconducting Quantum Processor, Phys. Rev. Lett. **122**, 110501 (2019).

[23] X.-Y. Luo, Y.-Q. Zou, L.-N. Wu, Q. Liu, M.-F. Han, M. K. Tey, and L. You, Deterministic entanglement generation from driving through quantum phase transitions, Science **355**, 620 (2017).

[24] F. Verstraete, M. M. Wolf, and J. I. Cirac, Quantum computation and quantum-state engineering driven by dissipation, Nat. Phys. **5**, 633 (2009).

[25] W. Song, W. Yang, J. An, and M. Feng, Dissipation-assisted spin squeezing of nitrogen-vacancy centers coupled to a rectangular hollow metallic waveguide, Opt. Express **25**, 19226 (2017).

[26] K. Stannigel, P. Rabl, and P. Zoller, Driven-dissipative preparation of entangled states in cascaded quantum-optical networks, New J. Phys. **14**, 063014 (2012).

[27] S.-l. Ma, P.-b. Li, A.-p. Fang, S.-y. Gao, and F.-l. Li, Dissipation-assisted generation of steady-state single-mode squeezing of collective excitations in a solid-state spin ensemble, Phys. Rev. A **88**, 013837 (2013).

[28] N. Lütkenhaus, J. I. Cirac, and P. Zoller, Mimicking a squeezed-bath interaction: Quantum-reservoir engineering with atoms, Phys. Rev. A **57**, 548 (1998).

[29] C. A. Muschik, E. S. Polzik, and J. I. Cirac, Dissipatively driven entanglement of two macroscopic atomic ensembles, Phys. Rev. A **83**, 052312 (2011).

[30] M. J. Kastoryano, F. Reiter, and A. S. Sørensen, Dissipative Preparation of Entanglement in Optical Cavities, Phys. Rev. Lett. **106**, 090502 (2011).

[31] Y.-H. Chen, W. Qin, and F. Nori, Fast and high-fidelity generation of steady-state entanglement using pulse modulation and parametric amplification, Phys. Rev. A **100**, 012339 (2019).

[32] E. G. Dalla Torre, J. Otterbach, E. Demler, V. Vuletic, and M. D. Lukin, Dissipative Preparation of Spin Squeezed Atomic Ensembles in a Steady State, Phys. Rev. Lett. **110**, 120402 (2013).

[33] Z. Jin, S. L. Su, and S. Zhang, Preparation of a steady entangled state of two nitrogen-vacancy centers by simultaneously utilizing two dissipative factors, Phys. Rev. A **100**, 052332 (2019).

[34] H. Krauter, C. A. Muschik, K. Jensen, W. Wasilewski, J. M. Petersen, J. I. Cirac, and E. S. Polzik, Entanglement Generated by Dissipation and Steady State Entanglement of Two Macroscopic Objects, Phys. Rev. Lett. **107**, 080503 (2011).

[35] D. Porras and J. J. García-Ripoll, Shaping An Itinerant Quantum Field Into a Multimode Squeezed Vacuum by Dissipation, Phys. Rev. Lett. **108**, 043602 (2012).

[36] S.-L. Su, X.-Q. Shao, H.-F. Wang, and S. Zhang, Scheme for entanglement generation in an atom-cavity system via dissipation, Phys. Rev. A **90**, 054302 (2014).

[37] W. Qin, A. Miranowicz, P.-B. Li, X.-Y. Lü, J. Q. You, and F. Nori, Exponentially Enhanced Light-Matter Interaction, Cooperativities, and Steady-State Entanglement Using Parametric Amplification, Phys. Rev. Lett. **120**, 093601 (2018).

[38] M. K. Bhaskar, D. D. Sukachev, A. Sipahigil, R. E. Evans, M. J. Burek, C. T. Nguyen, L. J. Rogers, P. Siyushev, M. H. Metsch, H. Park, F. Jelezko, M. Lončar, and M. D. Lukin, Quantum Nonlinear Optics with A Germanium-Vacancy Color Center in A Nanoscale Diamond Waveguide, Phys. Rev. Lett. **118**, 223603 (2017).

[39] Y. Zhou, B. Li, X.-X. Li, F.-L. Li, and P.-B. Li, Preparing multiparticle entangled states of nitrogen-vacancy centers via adiabatic ground-state transitions, Phys. Rev. A **98**, 052346 (2018).

[40] L. Childress, M. V. Gurudev Dutt, J. M. Taylor, A. S. Zibrov, F. Jelezko, J. Wrachtrup, P. R. Hemmer, and M. D. Lukin, Coherent dynamics of coupled electron and nuclear spin qubits in diamond, Science **314**, 281 (2006).

[41] M. W. Doherty, N. B. Manson, P. Delaney, F. Jelezko, J. Wrachtrup, and L. C. L. Hollenberg, The nitrogen-vacancy color center in diamond, Phys. Rep. **528**, 1 (2013).

[42] P.-B. Li and F. Nori, Hybrid quantum system with nitrogen-vacancy centers in diamond coupled to surface-phonon polaritons in piezomagnetic superlattices, Phys. Rev. Appl. **10**, 024011 (2018).

[43] B. Li, P.-B. Li, Y. Zhou, J. Liu, H.-R. Li, and F.-L. Li, Interfacing a topological qubit with a spin qubit in a hybrid quantum system, Phys. Rev. Appl. **11**, 044026 (2019).

[44] B. Pingault, J. N. Becker, C. H. H. Schulte, C. Arend, C. Hepp, T. Godde, A. I. Tartakovskii, M. Markham, C. Becher, and M. Atatüre, All-Optical Formation of Coherent Dark States of Silicon-Vacancy Spins in Diamond, Phys. Rev. Lett. **113**, 263601 (2014).

[45] J. N. Becker, J. Görlitz, C. Arend, M. Markham, and C. Becher, Ultrafast all-optical coherent control of single silicon vacancy colour centres in diamond, Nat. Commun. **7**, 13512 (2016).

[46] C. Weinzetl, J. Görlitz, J. N. Becker, I. A. Walmsley, E. Poem, J. Nunn, and C. Becher, Coherent Control and Wave Mixing in An Ensemble of Silicon-Vacancy Centers in Diamond, Phys. Rev. Lett. **122**, 063601 (2019).

[47] M.-A. Lemonde, V. Peano, P. Rabl, and D. G. Angelakis, Quantum state transfer via acoustic edge states in a 2d optomechanical array, New J. Phys. **21**, 113030 (2019).

[48] D. Chen, N. Zheludev, and W.-bo Gao, Building blocks for quantum network based on group-iv split-vacancy centers in diamond, Adv. Quantum Technol. **3**, 1900069 (2019).

[49] P.-B. Li, S.-Y. Gao, and F.-L. Li, Quantum-information transfer with nitrogen-vacancy centers coupled to a whispering-gallery microresonator, Phys. Rev. A **83**, 054306 (2011).

[50] F. Casola, T. van der Sar, and A. Yacoby, Probing condensed matter physics with magnetometry based on nitrogen-vacancy centres in diamond, Nat. Rev. Mater. **3**, 17088 (2018).

[51] D. Marcos, M. Wubs, J. M. Taylor, R. Aguado, M. D. Lukin, and A. S. Sørensen, Coupling Nitrogen-Vacancy Centers in Diamond to Superconducting Flux Qubits, Phys. Rev. Lett. **105**, 210501 (2010).

[52] P.-B. Li, Y.-C. Liu, S.-Y. Gao, Z.-L. Xiang, P. Rabl, Y.-F. Xiao, and F.-L. Li, Hybrid Quantum Device Based on NV Centers in Diamond Nanomechanical Resonators Plus Superconducting Waveguide Cavities, Phys. Rev. Appl. **4**, 044003 (2015).

[53] D. D. Awschalom, L. C. Bassett, A. S. Dzurak, E. L. Hu, and J. R. Petta, Quantum spintronics: Engineering and manipulating atom-like spins in semiconductors, Science **339**, 1174 (2013).

[54] Y.-Y. Lai, G.-D. Lin, J. Twamley, and H.-S. Goan, Single-nitrogen-vacancy-center quantum memory for a superconducting flux qubit mediated by a ferromagnet, Phys. Rev. A **97**, 052303 (2018).

[55] D. A. Golter, T. Oo, M. Amezcua, I. Lekavicius, K. A. Stewart, and H. Wang, Coupling a Surface Acoustic Wave to An Electron Spin in Diamond Via a Dark State, Phys. Rev. X **6**, 041060 (2016).

[56] J. R. Maze, A. Gali, E. Togan, Y. Chu, A. Trifonov, E. Kaxiras, and M. D. Lukin, Properties of nitrogen-vacancy centers in diamond: The group theoretic approach, New J. Phys. **13**, 025025 (2011).

[57] H. Bernien, L. Childress, L. Robledo, M. Markham, D. Twitchen, and R. Hanson, Two-Photon Quantum Interference from Separate Nitrogen Vacancy Centers in Diamond, Phys. Rev. Lett. **108**, 043604 (2012).

[58] A. Sipahigil, M. L. Goldman, E. Togan, Y. Chu, M. Markham, D. J. Twitchen, A. S. Zibrov, A. Kubanek, and M. D. Lukin, Quantum Interference of Single Photons from Remote Nitrogen-Vacancy Centers in Diamond, Phys. Rev. Lett. **108**, 143601 (2012).

[59] P.-B. Li, Z.-L. Xiang, P. Rabl, and F. Nori, Hybrid Quantum Device with Nitrogen-Vacancy Centers in Diamond Coupled to Carbon Nanotubes, Phys. Rev. Lett. **117**, 015502 (2016).

[60] T. Delord, L. Nicolas, Y. Chassagneux, and G. Hétet, Strong coupling between a single nitrogen-vacancy spin and the rotational mode of diamonds levitating in an ion trap, Phys. Rev. A **96**, 063810 (2017).

[61] P. Neumann, D. Twitchen, M. Markham, R. Kolesov, N. Mizuochi, J. Isoya, J. Achard, J. Beck, J. Tissler, V. Jacques, P. R. Hemmer, F. Jelezko, and J. Wrachtrup, Ultralong spin coherence time in isotopically engineered diamond, Nat. Mater. **8**, 383 (2009).

[62] L. J. Rogers, O. Wang, Y. Liu, L. Antoniuk, C. Osterkamp, V. A. Davydov, V. N. Agafonov, A. B. Filipovski, F. Jelezko, and A. Kubanek, Single Si-V^- Centers in Low-Strain Nanodiamonds with Bulklike Spectral Properties and Nanomanipulation Capabilities, Phys. Rev. Appl. **11**, 024073 (2019).

[63] Ö. O. Soykal, R. Ruskov, and C. Tahan, Sound-Based Analogue of Cavity Quantum Electrodynamics in Silicon, Phys. Rev. Lett. **107**, 235502 (2011).

[64] I. Lekavicius and H. Wang, Optical coherence of implanted silicon vacancy centers in thin diamond membranes, Opt. Express **27**, 31299 (2019).

[65] L. J. Rogers, K. D. Jahnke, M. H. Metsch, A. Sipahigil, J. M. Binder, T. Teraji, H. Sumiya, J. Isoya, M. D. Lukin, P. Hemmer, and F. Jelezko, All-Optical Initialization, Readout, and Coherent Preparation of Single Silicon-Vacancy Spins in Diamond, Phys. Rev. Lett. **113**, 263602 (2014).

[66] C. Hepp, T. Müller, V. Waselowski, J. N. Becker, B. Pingault, H. Sternschulte, D. Steinmüller-Nethl, A. Gali, J. R. Maze, M. Atatüre, and C. Becher, Electronic Structure of the Silicon Vacancy Color Center in Diamond, Phys. Rev. Lett. **112**, 036405 (2014).

[67] A. Gali and J. R. Maze, Ab initio study of the split silicon-vacancy defect in diamond: Electronic structure and related properties, Phys. Rev. B **88**, 235205 (2013).

[68] D. D. Sukachev, A. Sipahigil, C. T. Nguyen, M. K. Bhaskar, R. E. Evans, F. Jelezko, and M. D. Lukin, Silicon-Vacancy Spin Qubit in Diamond: A Quantum Memory Exceeding 10 ms with Single-Shot State Readout, Phys. Rev. Lett. **119**, 223602 (2017).

[69] E. Neu, C. Hepp, M. Hauschild, S. Gsell, M. Fischer, H. Sternschulte, D. Steinmüller-Nethl, M. Schreck, and C. Becher, Low-temperature investigations of single silicon vacancy color centres in diamond, New J. Phys. **15**, 043005 (2013).

[70] R. E. Evans, A. Sipahigil, D. D. Sukachev, A. S. Zibrov, and M. D. Lukin, Narrow-Linewidth Homogeneous Optical Emitters in Diamond Nanostructures via Silicon Ion Implantation, Phys. Rev. Appl. **5**, 044010 (2016).

[71] S. Meesala, Y.-I. Sohn, B. Pingault, L. Shao, H. A. Atikian, J. Holzgrafe, M. Gündoğan, C. Stavrakas, A. Sipahigil, C. Chia *et al.*, Strain engineering of the silicon-vacancy center in diamond, Phys. Rev. B **97**, 205444 (2018).

[72] K. V. Kepesidis, M.-A. Lemonde, A. Norambuena, J. R. Maze, and P. Rabl, Cooling phonons with phonons: Acoustic reservoir engineering with silicon-vacancy centers in diamond, Phys. Rev. B **94**, 214115 (2016).

[73] Y.-I. Sohn, S. Meesala, B. Pingault, H. A. Atikian, J. Holzgrafe, M. Gündoğan, C. Stavrakas, M. J. Stanley, A. Sipahigil, J. Choi, M. Zhang, J. L. Pacheco, J. Abraham, E. Bielejec, M. D. Lukin, M. Atatüre, and M. Lončar, Controlling the coherence of a diamond spin qubit through its strain environment, Nat. Commun. **9**, 2012 (2018).

[74] M.-A. Lemonde, S. Meesala, A. Sipahigil, M. J. A. Schuetz, M. D. Lukin, M. Loncar, and P. Rabl, Phonon Networks with Silicon-Vacancy Centers in Diamond Waveguides, Phys. Rev. Lett. **120**, 213603 (2018).

[75] X.-X. Li, B. Li, and P.-B. Li, Simulation of topological phases with color center arrays in phononic crystals, Phys. Rev. Research **2**, 013121 (2020).

[76] X. Wang and B. C. Sanders, Spin squeezing and pairwise entanglement for symmetric multiqubit states, Phys. Rev. A **68**, 012101 (2003).

[77] T. Lund-Hansen, S. Stobbe, B. Julsgaard, H. Thyrrestrup, T. Sünner, M. Kamp, A. Forchel, and P. Lodahl, Experimental Realization of Highly Efficient Broadband Coupling of Single Quantum Dots to a Photonic Crystal Waveguide, Phys. Rev. Lett. **101**, 113903 (2008).

[78] D. Dzsotjan, A. S. Sørensen, and M. Fleischhauer, Quantum emitters coupled to surface plasmons of a nanowire: A Green's function approach, Phys. Rev. B **82**, 075427 (2010).

[79] D. E. Chang, L. Jiang, A. V. Gorshkov, and H. J. Kimble, Cavity QED with atomic mirrors, New J. Phys. **14**, 063003 (2012).

[80] A. Asenjo-Garcia, J. D. Hood, D. E. Chang, and H. J. Kimble, Atom-light interactions in quasi-one-dimensional nanostructures: A Green's-function perspective, Phys. Rev. A **95**, 033818 (2017).

[81] E. Wolfe and S. F. Yelin, Certifying Separability in Symmetric Mixed States of n Qubits, and Superradiance, Phys. Rev. Lett. **112**, 140402 (2014).

[82] S. J. Masson and S. Parkins, Extreme spin squeezing in the steady state of a generalized Dicke model, Phys. Rev. A **99**, 023822 (2019).

[83] R. H. Dicke, Coherence in spontaneous radiation processes, Phys. Rev. **93**, 99 (1954).

[84] M. A. Stroscio, Y. M. Sirenko, S. Yu, and K. W. Kim, Acoustic phonon quantization in buried waveguides and resonators, J. Phys.: Condens. Matter **8**, 2143 (1996).

[85] J. R. Schrieffer and P. A. Wolff, Relation between the Anderson and Kondo Hamiltonians, Phys. Rev. **149**, 491 (1966).

[86] C. W. Gardiner, Driving a Quantum System with the Output Field from Another Driven Quantum System, Phys. Rev. Lett. **70**, 2269 (1993).

[87] H. J. Carmichael, Quantum Trajectory Theory for Cascaded Open Systems, Phys. Rev. Lett. **70**, 2273 (1993).

[88] M. Kitagawa and M. Ueda, Squeezed spin states, Phys. Rev. A **47**, 5138 (1993).

[89] D. J. Wineland, J. J. Bollinger, W. M. Itano, and D. J. Heinzen, Squeezed atomic states and projection noise in spectroscopy, Phys. Rev. A **50**, 67 (1994).

[90] D. J. Wineland, J. J. Bollinger, W. M. Itano, F. L. Moore, and D. J. Heinzen, Spin squeezing and reduced quantum noise in spectroscopy, Phys. Rev. A **46**, R6797(R) (1992).

[91] E. Wolfe and S. F. Yelin, Spin squeezing by means of driven superradiance, arXiv:1405.5288.

[92] J. Ma, X. Wang, C. P. Sun, and F. Nori, Quantum spin squeezing, Phys. Rep. **509**, 89 (2011).

[93] Y. Dong, X.-D. Chen, G.-C. Guo, and F.-W. Sun, Robust scalable architecture for a hybrid spin-mechanical quantum entanglement system, Phys. Rev. B **100**, 214103 (2019).

[94] X.-L. Dong and P.-B. Li, Multiphonon interactions between nitrogen-vacancy centers and nanomechanical resonators, Phys. Rev. A **100**, 043825 (2019).

[95] Q. Bin, X.-Y. Lü, F. P. Laussy, F. Nori, and Y. Wu, N-Phonon Bundle Emission via the Stokes Process, Phys. Rev. Lett. **124**, 053601 (2020).

[96] J. Wang, Y. Zhou, X. Zhang, F. Liu, Y. Li, K. Li, Z. Liu, G. Wang, and W. Gao, Efficient Generation of an Array of Single Silicon-Vacancy Defects in Silicon Carbide, Phys. Rev. Appl. **7**, 064021 (2017).

[97] D. M. Toyli, C. D. Weis, G. D. Fuchs, T. Schenkel, and D. D. Awschalom, Chip-scale nanofabrication of single spins and spin arrays in diamond, Nano Lett. **10**, 3168 (2010).